Improved spectral optical coherence tomography using optical frequency comb

Tomasz Bajraszewski, Maciej Wojtkowski*, Maciej Szkulmowski, Anna Szkulmowska, Robert Huber†, Andrzej Kowalczyk

Institute of Physics, Nicolaus Copernicus University, ul. Grudziadzka 5/7, 87-100 Torun, Poland
† Fakultät für Physik, Ludwig-Maximilians-Universität München, Munich, Germany.
**corresponding author: max@fizyka.umk.pl*

Abstract: We identify and analyze factors influencing sensitivity drop-off in Spectral OCT and propose a system employing an Optical Frequency Comb (OFC) to verify this analysis. Spectral Optical Coherence Tomography using a method based on an optical frequency comb is demonstrated. Since the spectrum sampling function is determined by the comb rather than detector pixel distribution, this method allows to overcome limitations of high resolution Fourier-domain OCT techniques. Additionally, the presented technique also enables increased imaging range while preserving high axial resolution. High resolution cross-sectional images of biological samples obtained with the proposed technique are presented.

OCIS codes: (110.4500) Optical coherence tomography; (110.4155) Multiframe image processing; (120.2230) Fabry-Perot; (170.3010) Image reconstruction techniques

References and Links

1. J. J. Kaluzny, A. Szkulmowska, T. Bajraszewski, M. Szkulmowski, B. J. Kaluzny, I. Gorczynska, P. Targowski, and M. Wojtkowski, "Retinal imaging by spectral optical coherence tomography," European journal of ophthalmology **17**, 238-245 (2007).
2. V. Christopoulos, L. Kagemann, G. Wollstein, H. Ishikawa, M. L. Gabriele, M. Wojtkowski, V. Srinivasan, J. G. Fujimoto, J. S. Duker, D. K. Dhaliwal, and J. S. Schuman, "In vivo corneal high-speed, ultra high-resolution optical coherence tomography," Archives of ophthalmology **125**, 1027-1035 (2007).
3. U. Schmidt-Erfurth, R. A. Leitgeb, S. Michels, B. Povazay, S. Sacu, B. Hermann, C. Ahlers, H. Sattmann, C. Scholda, A. F. Fercher, and W. Drexler, "Three-dimensional ultrahigh-resolution optical coherence tomography of macular diseases," Investigative ophthalmology & visual science **46**, 3393-3402 (2005).
4. V. J. Srinivasan, M. Wojtkowski, A. J. Witkin, J. S. Duker, T. H. Ko, M. Carvalho, J. S. Schuman, A. Kowalczyk, and J. G. Fujimoto, "High-definition and 3-dimensional imaging of macular pathologies with high-speed ultrahigh-resolution optical coherence tomography," Ophthalmology **113**, 2054 e2051-2014 (2006).
5. D. Huang, E. A. Swanson, C. P. Lin, J. S. Schuman, W. G. Stinson, W. Chang, M. R. Hee, T. Flotte, K. Gregory, C. A. Puliafito, and J. G. Fujimoto, "Optical coherence tomography," Science **254**, 1178-1181 (1991).
6. R. Leitgeb, C. K. Hitzenberger, and A. F. Fercher, "Performance of Fourier domain vs. time domain optical coherence tomography," Opt. Express **11**, 889-894 (2003).
7. J. F. de Boer, B. Cense, B. H. Park, M. C. Pierce, G. J. Tearney, and B. E. Bouma, "Improved signal-to-noise ratio in spectral-domain compared with time-domain optical coherence tomography," Opt. Lett. **28**, 2067-2069 (2003).
8. A. F. Fercher, C. K. Hitzenberger, G. Kamp, and S. Y. Elzaiat, "Measurement of Intraocular Distances by Backscattering Spectral Interferometry," Opt. Commun. **117**, 43-48 (1995).
9. M. Wojtkowski, R. Leitgeb, A. Kowalczyk, T. Bajraszewski, and A. F. Fercher, "In vivo human retinal imaging by Fourier domain optical coherence tomography," J. Biomed.Opt. **7**, 457-463 (2002).
10. S. R. Chinn, E. A. Swanson, and J. G. Fujimoto, "Optical coherence tomography using a frequency-tunable optical source," Opt. Lett. **22**, 340-342 (1997).
11. F. Lexer, C. K. Hitzenberger, A. F. Fercher, and M. Kulhavy, "Wavelength-tuning interferometry of intraocular distances," Appl. Opt. **36**, 6548-6553 (1997).
12. S. Yun, G. Tearney, J. de Boer, N. Iftimia, and B. Bouma, "High-speed optical frequency-domain imaging," Opt. Express **11**, 2953-2963 (2003).

#92342 - $15.00 USD Received 31 Jan 2008; revised 1 Mar 2008; accepted 7 Mar 2008; published 12 Mar 2008

13. T. Endo, Y. Yasuno, S. Makita, M. Itoh, and T. Yatagai, "Profilometry with line-field Fourier-domain interferometry," Opt. Express **13**, 695-701 (2005).
14. B. Grajciar, M. Pircher, A. Fercher, and R. Leitgeb, "Parallel Fourier domain optical coherence tomography for in vivo measurement of the human eye," Opt. Express **13**, 1131-1137 (2005).
15. Y. Nakamura, S. Makita, M. Yamanari, M. Itoh, T. Yatagai, and Y. Yasuno, "High-speed three-dimensional human retinal imaging by line-field spectraldomain optical coherence tomography," Opt. Express **15**, 7103-7116 (2007).
16. M. Wojtkowski, V. J. Srinivasan, T. H. Ko, J. G. Fujimoto, A. Kowalczyk, and J. S. Duker, "Ultrahigh-resolution, high-speed, Fourier domain optical coherence tomography and methods for dispersion compensation," Opt. Express **12**, 2404-2422 (2004).
17. M. A. Choma, M. V. Sarunic, C. H. Yang, and J. A. Izatt, "Sensitivity advantage of swept source and Fourier domain optical coherence tomography," Opt. Express **11**, 2183-2189 (2003).
18. S. H. Yun, G. J. Tearney, J. F. de Boer, and B. E. Bouma, "Pulsed-source and swept-source spectral-domain optical coherence tomography with reduced motion artifacts," Opt. Express **12**, 5614-5624 (2004).
19. R. Huber, D. C. Adler, and J. G. Fujimoto, "Buffered Fourier domain mode locking: Unidirectional swept laser sources for optical coherence tomography imaging at 370,000 lines/s," Opt. Lett. **31**, 2975-2977 (2006).
20. B. Cense, N. A. Nassif, T. C. Chen, M. C. Pierce, S.-H. Yun, B. H. Park, B. E. Bouma, G. J. Tearney, and J. F. de Boer, "Ultrahigh-resolution high-speed retinal imaging using spectral-domain optical coherence tomography," Opt. Express **12**, 2435-2447 (2004).
21. M. Wojtkowski, T. Bajraszewski, I. Gorczynska, P. Targowski, A. Kowalczyk, W. Wasilewski, and C. Radzewicz, "Ophthalmic imaging by spectral optical coherence tomography," Am. J. Ophthalmol. **138**, 412-419 (2004).
22. H. Lim, J. F. De Boer, B. H. Park, E. C. W. Lee, R. Yelin, and S. H. Yun, "Optical frequency domain imaging with a rapidly swept laser in the 815-870 nm range," Opt. Express **14**, 5937-5944 (2006).
23. V. J. Srinivasan, R. Huber, I. Gorczynska, J. G. Fujimoto, J. Y. Jiang, P. Reisen, and A. E. Cable, "High-speed, high-resolution optical coherence tomography retinal imaging with a frequency-swept laser at 850 nm," Opt. Lett. **32**, 361-363 (2007).
24. D. C. Adler, Y. Chen, R. Huber, J. Schmitt, J. Connolly, and J. G. Fujimoto, "Three-dimensional endomicroscopy using optical coherence tomography," Nature Photonics **1**, 709-716 (2007).
25. P. Targowski, M. Wojtkowski, A. Kowalczyk, T. Bajraszewski, M. Szkulmowski, and I. Gorczynska, "Complex spectral OCT in human eye imaging in vivo," Opt. Commun. **229**, 79-84 (2004).
26. M. Wojtkowski, A. Kowalczyk, R. Leitgeb, and A. F. Fercher, "Full range complex spectral optical coherence tomography technique in eye imaging," Opt. Lett. **27**, 1415-1417 (2002).
27. A. Bachmann, R. Leitgeb, and T. Lasser, "Heterodyne Fourier domain optical coherence tomography for full range probing with high axial resolution," Opt. Express **14**, 1487-1496 (2006).
28. Y. Yasuno, S. Makita, T. Endo, G. Aoki, M. Itoh, and T. Yatagai, "Simultaneous B-M-mode scanning method for real-time full-range Fourier domain optical coherence tomography," Appl. Opt. **45**, 1861-1865 (2006).
29. R. K. Wang, "In vivo full range complex Fourier domain optical coherence tomography," Appl. Phys. Lett. **90**, 054103 (2007).
30. Z. Wang, Z. Yuan, H. Wang, and Y. Pan, "Increasing the imaging depth of spectral-domain OCT by using interpixel shift technique," Opt. Express **14**, 7014-7023 (2006).
31. Y. Yasuno, V. D. Madjarova, S. Makita, M. Akiba, A. Morosawa, C. Chong, T. Sakai, K.-P. Chan, M. Itoh, and T. Yatagai, "Three-dimensional and high-speed swept-source optical coherence tomography for in vivo investigation of human anterior eye segments," Opt. Express **13**, 10652-10664 (2005).
32. B. Hyle Park, M. C. Pierce, B. Cense, S.-H. Yun, M. Mujat, G. J. Tearney, B. E. Bouma, and J. F. de Boer, "Real-time fiber-based multi-functional spectral domain optical coherence tomography at 1.3 μm," Opt. Express **13**, 3931-3944 (2005).
33. H. Y. Ryu, H. S. Moon, and H. S. Suh, "Optical frequency comb generator based on actively mode-locked fiber ring laser using an acousto-optic modulator with injection-seeding," Opt. Express **15**, 11396-11401 (2007).
34. E. Gotzinger, M. Pircher, R. Leitgeb, and C. K. Hitzenberger, "High speed full range complex spectral domain optical coherence tomography," Opt. Express **13**, 583-594 (2005).
35. B. Baumann, M. Pircher, E. Gotzinger, and C. K. Hitzenberger, "Full range complex spectral domain optical coherence tomography without additional phase shifters," Opt. Express **15**, 13375-13387 (2007).

1. Introduction

Optical Coherence Tomography (OCT) is a non-contact and non-invasive high-resolution technique for imaging of partially transparent objects. It has found a wide spectrum of applications in biomedical imaging, especially in ophthalmology [1-4]. OCT enables reconstructing information about the depth structure of a sample using interferometry of

#92342 - $15.00 USD Received 31 Jan 2008; revised 1 Mar 2008; accepted 7 Mar 2008; published 12 Mar 2008

temporally low coherent light. There are two variants of OCT techniques depending on the detection system: Time-domain (TdOCT) and Frequency-domain (FdOCT). TdOCT was proposed by Huang et al. in 1991 [5]. FdOCT provides significant improvement of imaging speed and detection sensitivity as compared to TdOCT [6, 7]. FdOCT enables reconstructing the depth resolved scattering profile at a certain point on the sample from a modulation of the optical spectrum caused by interference of light beams [8] and can be performed in two ways: either the spectrum is measured by a spectrometer (Spectral OCT) [8, 9] or in a configuration including a tunable laser and a single dual balanced photodetector (Swept source OCT) [10-12]. In Spectral OCT (SOCT) a light source with broad spectral bandwidth (~100 nm) is used in combination with a spectrometer and a line or array of photo-sensitive detectors [9, 13-15]. SOCT instruments achieve shot noise limited detection [6] with a speed up to 50k Ascans/s and an axial resolution as high as 2 μm in tissue [16]. The second method, Swept Source OCT (SS-OCT), employs a rapidly tunable laser [17, 18]. SS-OCT usually operates at speeds comparable to SOCT. However, the recent introduction of Fourier Domain Mode Locking (FDML) enabled a dramatic increase in imaging speed of SS-OCT up to 370k A-scans/s [19]. The axial resolution of most SS-OCT systems is on the order of 10 μm in tissue and doesn't match high resolution SOCT systems. Due to the high imaging speed, FdOCT systems enable the acquisition of three dimensional image data *in-vivo* which is especially beneficial for numerous ophthalmic imaging applications [20, 21]. Currently, the high axial resolution of 2-3 μm of SOCT systems in the 850nm range can not be matched by SS-OCT systems. Lim et al. [22] reported SS-OCT operating at around 840 nm with speed up to 43.2k A-scans/s and axial resolution of 13 μm in air. Different SS-OCT operating at 850 nm was described by Srinivasan et al. [23]. The system operates at 16k A-scans/s and achieves axial resolution of 7 μm. At 1300 nm center wavelength, high speed OCT instrument based on swept source enables 5-7 μm axial resolution [24].

In spite of the resolution advantage of SOCT instruments, limitations in the imaging range due to a finite resolution of the spectrometer represent a major drawback. In general the effect of the depth dependent sensitivity drop together with mirror-conjugate images [6] reduces the total imaging range of both Fourier-domain techniques but is more significant in SOCT. There are several techniques allowing minimizing these shortcomings. These techniques are based on the reconstruction of the complex interferometric signals [25-29] and thus eliminating mirror-images caused by Fourier transformation of real valued signals, increasing the effective ranging depth by a factor of two. A different method for doubling the imaging range was proposed by Wang et al. [30]. They propose an interpixel shift technique in order to effectively double the number of collected samples. However, the method is based on mechanical movement of the detector making this approach comparably slow.

In this contribution we identify and analyze factors influencing sensitivity drop-off in Spectral OCT and propose a system employing an Optical Frequency Comb (OFC) to verify this analysis. It appears that OFC effectively reduces the depth dependent drop of sensitivity and might be considered as a method improving performance of SOCT. The Optical Frequency Comb is considered to be a spectrum consisting discrete and equidistantly distributed optical frequency components created either by optical filtration of spectrally broadband light or generated as a laser optical comb. This new method enables more flexible change of the measurement depth without the need of introducing any changes in the SOCT device. Additionally, in the presented technique samples of interference signal extracted by an optical comb spectrum are equidistantly distributed in optical frequencies, thus completely avoiding the necessity of wavelength to frequency rescaling [9, 31, 32].

2. Phenomena deteriorating the depth dependent sensitivity in SOCT

A significant technical weakness of SOCT is the depth dependent signal drop [9, 16, 30]. Spectral OCT devices comprise the spectrographic set-up, which enables the spatial separation of light with different $k(\zeta)$, where ζ denotes a spatial coordinate corresponding to the direction determined by the distribution of photo-sensitive elements of the detector. In a simplified SOCT experiment with a mirror as an object, the interference signal can be

#92342 - $15.00 USD Received 31 Jan 2008; revised 1 Mar 2008; accepted 7 Mar 2008; published 12 Mar 2008

represented by a cosine function of wave number k multiplied by the doubled optical path-difference Δz between the two arms of the Michelson interferometer

$$I(\zeta) = 2G(\zeta)\left[1+\cos\left(2k(\zeta)\Delta z\right)\right]. \tag{1}$$

We assume here equal back reflected light intensities from the reference and sample arm. In an ideal case of the cosine function, which infinitely spreads in k-space, the Fourier transform yields two Dirac deltas $\delta(z \pm \Delta z)$ located at Δz and $-\Delta z$. In a real experiment, the interference signal is limited by the spectral bandwidth $G[k(\zeta)] \equiv G(\zeta)$ of the light source (Fig. 1(a)). Thus, in the conjugate space the Dirac deltas are convolved with the coherence function $\Gamma(z)$:

$$\left|FT\left\{I(\zeta)\right\}\right| = DC + \left|\Gamma(z)\right| \otimes \delta\left(z \pm \Delta z\right), \tag{2}$$

where DC indicates low frequency components of the spectral fringe signal called also as autocorrelation function [9], and $\Gamma(z)$ is linked to the spectral density $G(\zeta)$ according to Wiener-Khinchin theorem. Since the spectrum is registered by an array or matrix of photo-sensitive elements, interference fringes are additionally convolved with the *rect* function $\Pi_{\delta\zeta/2}(\zeta)$ representing a single photo-sensitive element of the detector with $\delta\zeta$ as a width of a single pixel. The Fourier transform of the *rect* function is a *sinc* function − Fig. 1(b).

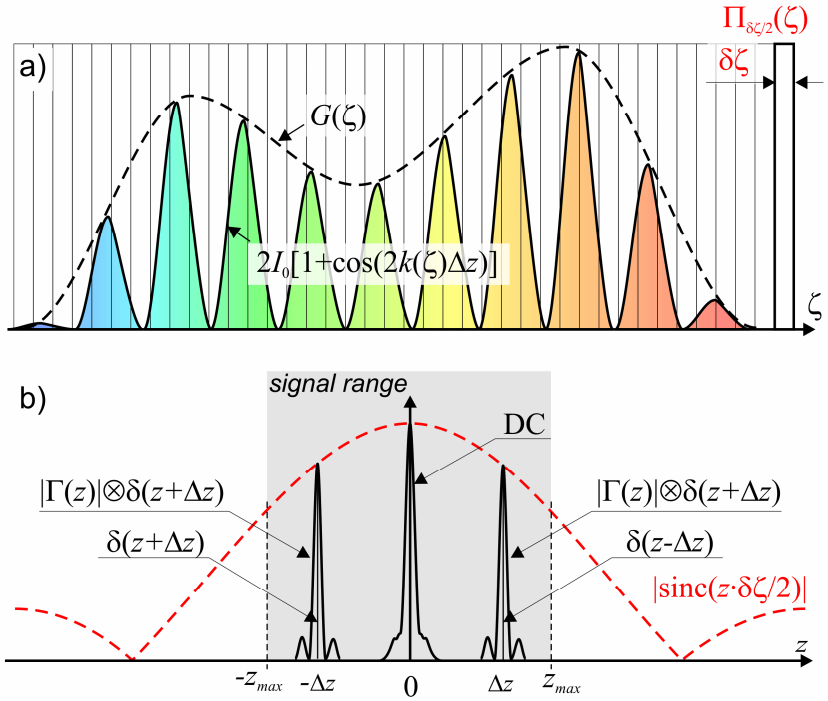

Fig. 1. a) Simulation of the interferometric signal; dotted line: spectrum of the light source $G(\zeta)$; solid line: modulation due to interference; b) corresponding Fourier transform after integration within the "pixel" width $\delta\zeta$.

In an SOCT system the width of the *sinc* function depends on $\delta\zeta$ and it is related to the decrease of the interference fringes visibility as a function of increasing modulation frequency. The limited resolution of a spectrometer causes a suppression of amplitudes of high frequency components of the spectral fringe signal.

There are additional significant factors affecting the signal in SOCT devices. Usually the spectrometer used in SOCT comprises a diffraction grating followed by a lens and CCD or CMOS array. The spectrometer enables to obtain a spectrum evenly sampled in wavelength, not in wave number k-space:

#92342 - $15.00 USD Received 31 Jan 2008; revised 1 Mar 2008; accepted 7 Mar 2008; published 12 Mar 2008

$$\zeta \propto \lambda \Rightarrow k(\zeta) \propto \frac{2\pi}{\zeta}. \tag{3}$$

As the structural information is encoded in frequencies of *k* dependent spectral fringes, two problems arise. Both are related to variable spectral width (in wave numbers) of an individual pixel and simultaneously to a spectral separation between two adjacent pixels. Both of these effects cause that the short wavelength part of the spectrum is more sparsely sampled (in *k*) than the long wavelength part. This means that high frequencies of the spectral fringes are aliased and irretrievably lost in the part of the spectrum while the rest of the signal can remain within the Nyquist limit. We called this effect as *partial aliasing*. Figure 2 shows a simulated decrease of the signal caused by partial aliasing as a function of normalized optical path difference for different spectral spans. The signal was simulated for each optical path difference, numerically recalculated to *k*-space and Fourier transformed. The amplitude of the resulted point-spread function (PSF) was drawn on the graph. For wider spectral spans, the effect appears at smaller optical path differences.

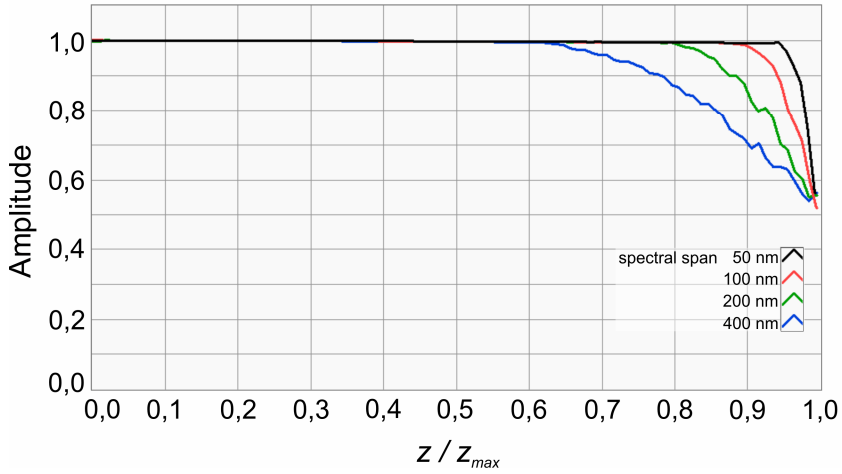

Fig. 2. SOCT amplitudes of the axial Point-Spread Function depending on the axial position for different optical spectral spans. In the presented simulation the cosine signal generated in λ-space is numerically recalculated to *k*-space. The simulation does not include the signal integration within the particular pixels. The amplitudes are normalized to the value corresponding to z = 0 and the z scale is normalized to the maximal optical path difference z_{max} for the specific spectral span.

As it could be expected the amplitude of the PSFs is affected strongly by the partial aliasing for higher frequencies of the spectral fringe signal (higher optical path differences). Additionally this effect increases with the spectral bandwidth (higher axial resolution of SOCT system). In our simulation the maximal loss of signal power caused by the effect reaches 5.2 dB at the end of axial measurement range regardless of spectral span.

Another important factor decreasing the SOCT signal is the electronic interpixel crosstalk present in CCD detectors. Due to this effect, the charge from a particular pixel is spread over the neighboring pixels, what causes additional degradation of the spectrometer resolution. The depth dependent signal loss function associated with this effect can be experimentally found by illuminating a single pixel of the camera with a focal spot smaller than the dimension of the pixel. The Fourier transformation of the CCD detector response (Fig. 3) will provide a function describing the fringe visibility loss.

#92342 - $15.00 USD Received 31 Jan 2008; revised 1 Mar 2008; accepted 7 Mar 2008; published 12 Mar 2008

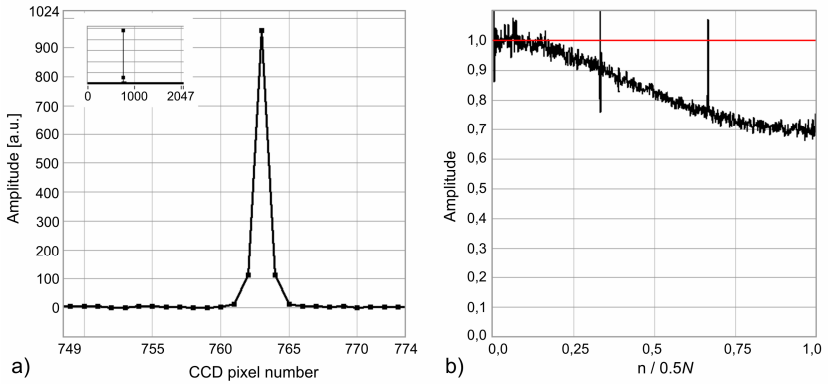

Fig. 3. Analysis of interpixel crosstalk influencing the performance of the SOCT system. a) a part of the signal registered by a line scan CCD detector (inset shows the total signal) illuminated with a laser beam tightly focused onto a single pixel. b) Fourier transform of the intensity signal on a linear scale corresponding to the fringe visibility loss due to the interpixel crosstalk. The spikes visible on the Fourier transform graph are caused by coherent noise introduced by the internal electronics of the CCD detector.

We analyzed the influence of the interpixel crosstalk effect in a high speed line scan CCD camera (Atmel Aviiva M4 CL2014, 14x14 μm pixel size) using a beam of a single mode, monochromatic laser at 830 nm, collimated by a microscopic objective OLYMPUS 20X, expanded in a telescopic system with magnification of 5x and focused onto a single pixel by a Spindler&Hoyer focusing objective with a focal length of 30 mm. The calculated diameter of the spot size at the level of e^{-2} of the intensity profile is 5.3 μm. The visibility of the registered fringes due to the interpixel crosstalk effect drops to 0.7 which gives an additional −3,1 dB signal power loss. In a real spectrometer it is very hard to distinguish between the interpixel crosstalk effect and the decrease of the spectral resolution caused by the finite size of the focal spot size. In order to analyze these effects jointly we repeated above mentioned experiment by using different focusing lenses but keeping the same entrance beam diameter. A logarithmic plot of the maximal sensitivity drop (corresponding to the Nyquist frequency after Fourier transformation) as a function of focal length is presented in Fig. 4. The black solid line corresponds to the calculated values of sensitivity drop caused only by the influence of the finite focal spot size for a given CCD pixel size (14 μm). Once the focal spot size is getting bigger than the pixel width, the signal (fringe visibility) starts to decrease. The experimental data roughly follows the theoretical curve, but the deviation from the curve shape is probably due to the imperfect optical system which does not guarantee the ideal focal spot. However, constant −4 dB offset between the theoretical curve and the measured points is clearly visible. This offset corresponds to the previously measured value of the interpixel crosstalk. This experiment also shows that the spectral fringe signal is always convolved with the interpixel crosstalk described by the function *Crosstalk*(ζ) and it is also convolved with the focal spot function *SpotSize*(ζ). For the sake of simplicity we can analyze these two effects jointly describing them as a single function: $B(\zeta) = Crosstalk(\zeta) \otimes SpotSize(\zeta)$, where ⊗ denotes convolution operation.

All effects, including the rectangular characteristic of a single pixel $\Pi_{\delta\zeta/2}(\zeta)$, partial aliasing $A(\zeta)$, the finite focal spot size and interpixel crosstalk $B(\zeta)$, deteriorate the resolution of the spectrometer and all of them are convolved with the spectral fringe signal $I(\zeta)$:

$$I_{reg}(\zeta) = \left[\Pi(\zeta) \otimes B(\zeta) \otimes A(\zeta)\right] \otimes I(\zeta), \tag{4}$$

where $I_{reg}(\zeta)$ is the registered spectral fringe signal. The Fourier transform of the spectral fringes $I(\zeta)$ will be multiplied with the Fourier transform of the functions $\Pi_{\delta\zeta/2}(\zeta)$, $B(\zeta)$ and $A(\zeta)$. Figure 5 shows a linear plot of $FT\{\Pi_{\delta\zeta/2}(\zeta)\}$, $FT\{B(\zeta)\}$, $FT\{A(\zeta)\}$ and $FT\{I_{reg}(\zeta)\}$ found theoretically.

#92342 - $15.00 USD Received 31 Jan 2008; revised 1 Mar 2008; accepted 7 Mar 2008; published 12 Mar 2008

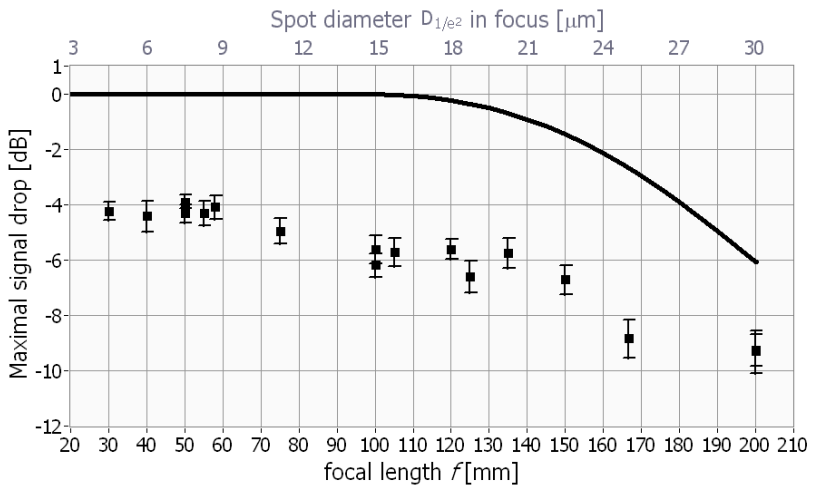

Fig. 4. Points representing the maximal signal drop (registered at the end of the axial measurement range) as a function of focal length of the imaging lens measured and calculated for a CCD camera model Aviiva M4 CL2014 from Atmel. The black solid line shows the calculated signal drop caused by the finite spot size at the detector.

On the same plot the experimental data show the measured normalized depth dependent sensitivity drop of the SOCT system.

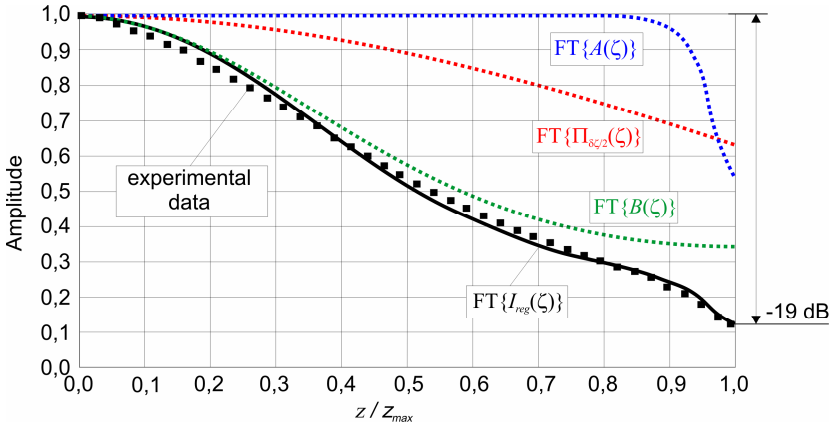

Fig. 5. Reduction of fringes visibility as a function of optical path difference z. The plot shows separate effects: finite pixel size (red) calculated theoretically, aliasing (blue) found by simulation and spot size (green) determined by experiment prformed for the focal length of the spectrometer objective f= 200 mm. The solid black line is the cumulative occurrence. The squares represent experimental data. The signal power drop can be as high as −19 dB.

3. Implementation of the optical frequency comb in SOCT device

In order to increase the spectral resolving power of the detection unit in SOCT we propose to use a light source, which generates a discrete distribution of optical frequencies (called optical frequency comb) instead of continuous broadband light. In order to give a proof of concept of this idea we constructed passive optical frequency comb generator comprising a broadband light source and a fiber Fabry-Perot (F-P) filter. The real interference signal $I(k)$ is thus multiplied by a transmission function T_{FPI} of the F-P filter

$$I_{OFC}(k) = T_{FPI}(k) \cdot I(k) . \qquad (5)$$

#92342 - $15.00 USD Received 31 Jan 2008; revised 1 Mar 2008; accepted 7 Mar 2008; published 12 Mar 2008

The function $T_{FPI}(k)$ can be expressed as a convolution of the Cauchy (or Lorentz) distribution function and Dirac comb $D_{\pi d}(k)$:

$$T_{FPI} = \frac{\pi T^2}{d(1-R^2)} L(k;\gamma) \otimes D_{\pi/d}(k), \tag{6}$$

where T and R are transmission and reflection coefficients of the F-P interferometer surfaces respectively, γ is defined as $\gamma = -(2d)^{-1}\ln(R)$, d is separation between two surfaces in F-P interferometer which is related to $FSR = c/(2d)$ assuming an air-gap in the F-P, and $L(k;\gamma) = \gamma[\pi(\gamma^2 + k^2)]^{-1}$. Combining Eq. (5) and Eq. (6) we obtain:

$$I_{OFC}(k) = \frac{\pi T^2}{d(1-R^2)} L(k;\gamma) \otimes D_{\pi/d}(k) \cdot I(k). \tag{7}$$

Calculating Fourier transform of the Eq. (7) we obtain

$$FT\{I_{OFC}(k)\} \equiv G^{OFC}(z) = \frac{\sqrt{2\pi}T^2}{(1-R^2)} \exp\left(\frac{\pi}{d}\ln(R)|z|\right) \cdot D_{2d}(z) \otimes g(z), \tag{8}$$

where $g(z)$ denotes the Fourier transform of $I(k)$ and describes the object structure. From the Eq. (8) one can see that the object image is periodically repeated with the period $2d$ in z-space. The signal drop within the imaging range is determined by an exponential function and depends on the reflectivity R of the mirrors in the Fabry-Perot interferometer. To get advantage of using a comb in SOCT, one should ensure that any two adjacent comb lines illuminating a CCD detector are clearly separated. Such an arrangement strongly reduces the influence of the interpixel crosstalk and the limited spot size, since a signal from a particular line of the comb does not disturb the signal of the adjacent lines. Moreover, the line width BW of the optical frequency comb is chosen to be much smaller than the spectral range covered by a single pixel ($BW << \delta k$). Thus the signal drop caused by a *sinc* function corresponding to the pixel size is replaced by the Fourier transform of the shape of the single comb line. Therefore, the corresponding sensitivity loss is less significant.

4. SOCT Multiplexing technique using tunable optical frequency comb generator

In our experiments we selected $FSR = 4\,\delta k$, so peaks of the optical frequency comb are clearly separated. The exact positions of the comb peaks on the CCD detector are then used to decode the interference signal. Each sample of the spectral fringe pattern is obtained from the part of the detector illuminated by a particular comb line. Thus the resulting interference signal is compound with samples presented directly in k domain. This, however, gives the number of reconstructed signal points to be four times smaller than the number of pixels of the detector, what results in four-fold reduction of imaging range (area with $M = 1$ on Fig. 6). To overcome this drawback, we propose to use, so called, multiplexing technique. In this new method, the interference pattern is sampled M times at a given point of the object. This can be mathematically expressed by:

$$G_m(j) = \begin{cases} G^{OFC}(j), & j = l \cdot M + m \\ 0, & j \neq l \cdot M + m \end{cases} \tag{9}$$

where j indexes points of the resulting multiplexed signal, l indexes the samples of a single comb record and it changes from 0 to the number of detected comb lines, and m indicates particular comb measurement and changes from 0 to $M - 1$. Each set of samples is obtained by shifting the comb over the CCD detector by a fraction of the FSR. The comb is effectively shifted by changing the gap width d inside the F-P interferometer. Such change slightly alters

#92342 - $15.00 USD Received 31 Jan 2008; revised 1 Mar 2008; accepted 7 Mar 2008; published 12 Mar 2008

the *FSR*, however, this change is relatively small with respect to changes of the comb line positions (different set of wavelengths are transmitted by the F-P interferometer). During postprocessing, a multiplexed signal, $G^{MUX}(j)$ is then obtained by summation operation

$$G^{MUX}(j) = \sum_{m=0}^{M-1} G_m(j). \tag{10}$$

Since the $G^{MUX}(j)$ is represented in *k*-space, it can be directly Fourier transformed to provide a single A-scan. For the special case of $M = 1$, there is no multiplexing technique and a single A-scan is obtained from single set of samples. To get the imaging range similar to that obtained by standard SOCT system, four measurements per single axial scan ($M = 4$ on Fig. 4) should be performed with the consecutive shifts of *FSR*/4. To reconstruct the final interference signal, four spectral fringes have to be multiplexed.

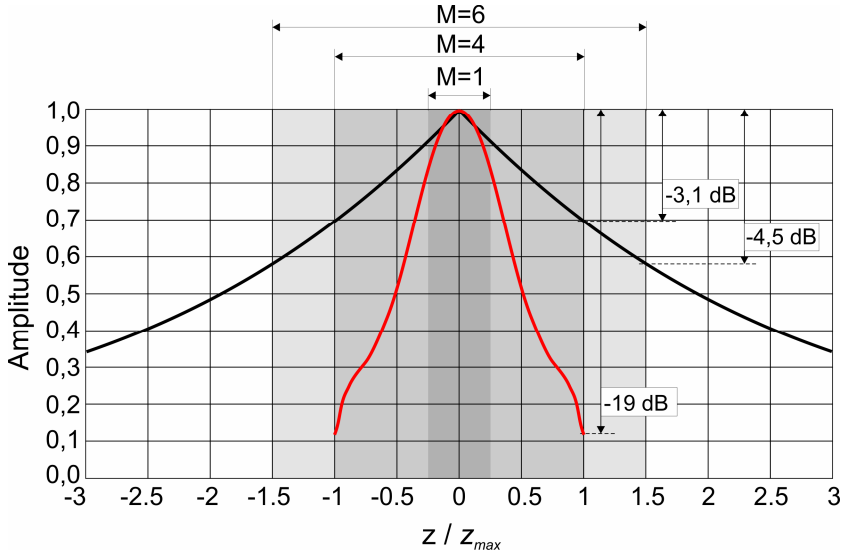

Fig. 6. Comparison of theoretical sensitivity drop in standard (red) and improved (black) SOCT, as a function of reduced imaging range. Both curves were calculated with parameters related to the experiment. Gray areas correspond to imaging ranges for standard SOCT and multiplexing method with different *M*

Figure 6 compares the sensitivity drop of standard SOCT (same as the black line in Fig. 5) with the calculated exponential function describing the signal drop due to convolution of the fringes with the comb shape. Comb lines are assumed to illuminate every fourth pixel of the CCD camera. Maximal imaging depth, as compared to the standard SOCT, is reduced four times for $M = 1$, is the same for $M = 4$, and is 50 % wider for $M = 6$. The signal loss at the specific maximal depth calculated for the method with $M = 4$ is −3.1 dB, and with $M = 6$ is −4.5 dB. The effective number of samples can be higher than the number of pixels of the detector resulting in expansion of the imaging depth. It must be noted, that simple increase of number of pixels in CCD camera in standard SOCT will theoretically increase imaging depth, but because of dramatic loss of sensitivity, in practice there will be no improvement in imaging range.

5. Apparatus and results

Figure 7 shows a schematic drawing of the experimental setup as a demonstration system. The light source BLS (Broadlighter T840, Superlum, Moscow), a broad spectrum, optical isolator OI and tunable fiber Fabry-Perot interferometer FPI (Micron Optics, *FSR* = 89 GHz, *BW* = 1.62 GHz, *Finesse* = 55) form an optical frequency comb generator OFCG. The light

#92342 - $15.00 USD Received 31 Jan 2008; revised 1 Mar 2008; accepted 7 Mar 2008; published 12 Mar 2008

from the OFCG enters the Michelson interferometer of the SOCT device. The OFC signal registered by a spectrometer is shown in Fig. 6(b). The FPI is driven with a voltage staircase waveform to perform experiments with multiplexing final interference signal. A specially designed electronic unit DRV generates the signals for an acoustic amplifier (AMP – Tonsil, Poland), for the galvo-scanner S of the imaging setup (Cambridge Technology, UK) and for the trigger of the CCD camera (Atmel, USA).

The power of the light at the object was 25 μW due to the high power loss at the FPI equal to 19 dB. The sensitivity of the SOCT system with the OFC, measured around zero path difference, at 25 μW power of light and 150 μs exposure time, was 92 dB. The axial resolution of SOCT system was 5 μm in air (~3,5 μm in tissue) in all experiments.

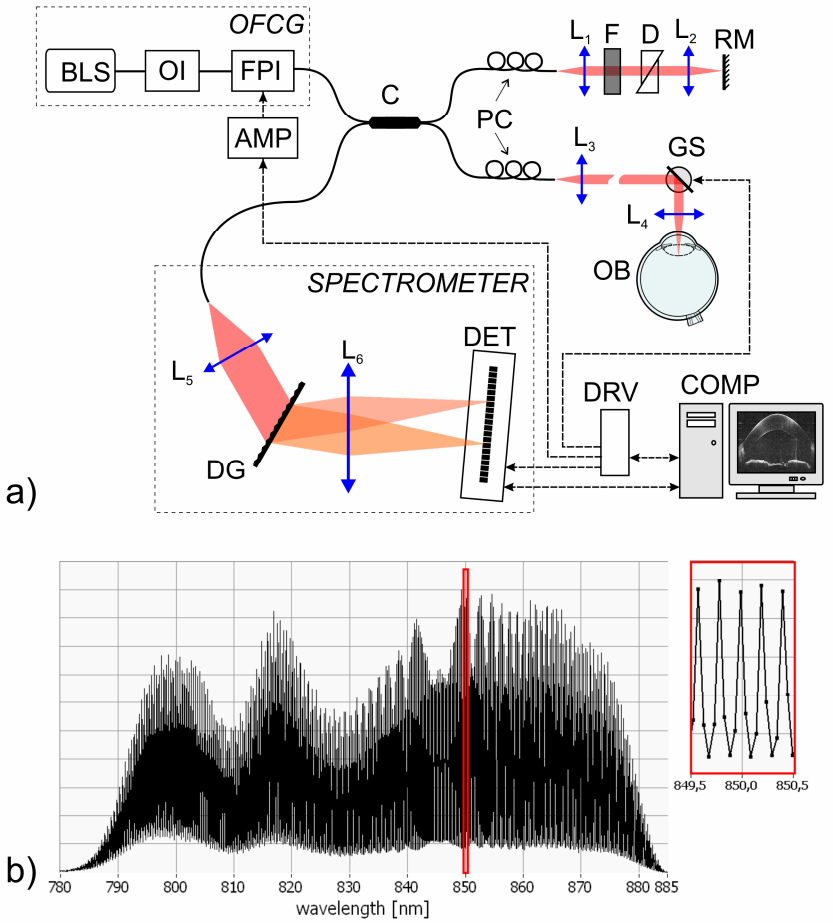

Fig. 7. a) SOCT system setup using an Optical Frequency Comb generator OFCG; b) optical frequency comb signal registered by a spectrometer. BLS – broad band light source, OI – optical isolator, FPI – tunable Fabry-Perot interferometer, AMP – amplifier, C – coupler, PC-polarization controllers, $L_{1\text{-}6}$ – lenses, F – neutral density filter, D – prism pair for dispersion compensation, RM – reference mirror, GS – galvoscanner, OB-object, DG – diffraction grating, DRV – control unit. Note, that the modulation of the comb is not 100%. It is due to the phenomena deteriorating the spectrometer resolution described in section 2

Figure 8 shows images of *in vivo* cornea and retina of a human eye using the described method for $M = 1$ (i.e. without multiplexing). Both objects are imaged with high axial resolution, however the imaging range is just equal to the depth of the object.

#92342 - $15.00 USD Received 31 Jan 2008; revised 1 Mar 2008; accepted 7 Mar 2008; published 12 Mar 2008

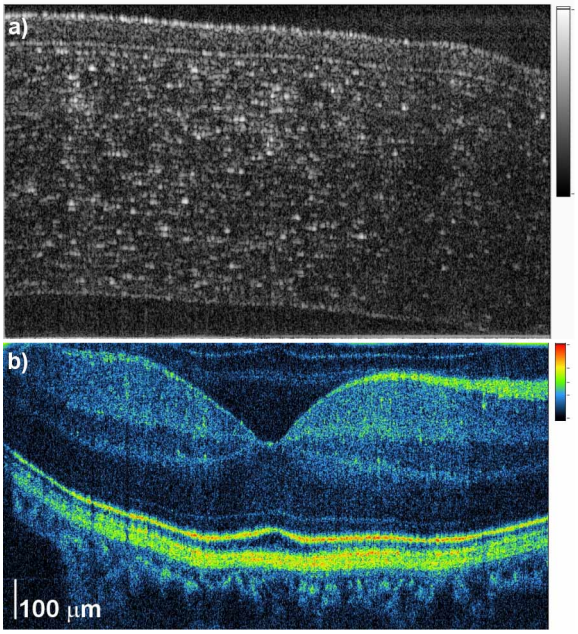

Fig. 8. Cross-sectional images of human eye *in vivo* obtained by the SOCT system using optical frequency comb for M = 1. a) cornea b) foveal region of the retina

To avoid the limited imaging range, we performed experiments using multiplexing technique for $M = 4$ and $M = 6$ and compared with the result of the standard SOCT technique. The multiplexing method for $M = 4$ enables to image the same imaging range as a standard system while for $M = 6$ the imaging range expands 1.5 times.

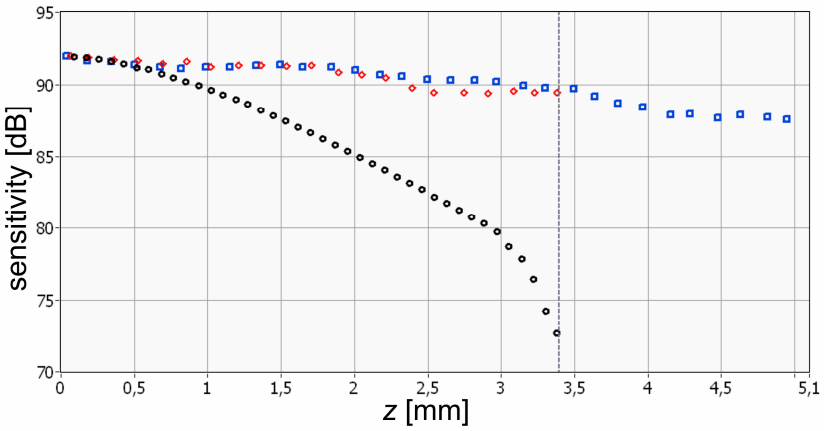

Fig. 9. SOCT sensitivity drop as a function of optical path difference for standard SOCT (black dots) and SOCT using optical frequency comb in multiplexed measurements for $M = 4$ (red rhombs) and $M = 6$ (blue squares)

Figure 9 shows results of measurements of depth-dependent sensitivity. The predicted value of the maximal signal drop for the multiplexing method for $M = 4$ is −3.1 dB and for $M = 6$ is −4.5 dB and are in agreement with the experimental results. This experiment shows that the described method gains approximately 14 dB sensitivity at the end of the axial measurement range (3.4 mm) compared to the standard technique. It also shows that it is possible to extend the measurement range to 5 mm with decrease of sensitivity less than 5 dB.

#92342 - $15.00 USD Received 31 Jan 2008; revised 1 Mar 2008; accepted 7 Mar 2008; published 12 Mar 2008

To demonstrate the applicability of the multiplexing method, we examined the anterior chamber of porcine eye *in vitro*. Figure 10(a) shows a result obtained by standard SOCT technique. With this method we could image only a part of the anterior segment due to the limited imaging range as well as reduced sensitivity. Figure 10(b) displays the effect of the multiplexing method with $M = 4$ to obtain approximately the same axial measurement range. Because of the increased sensitivity the folded image of the iris became visible. In order to image the entire anterior segment without iris folding we performed multiplexing technique for $M = 6$ (Fig. 10(c)).

Since our preliminary setup of the OFCG reduces the power of the object beam to 25 μW, the power of light illuminating the eye for a standard SOCT experiment was also attenuated to this level to ensure comparable conditions for both experiments. To partially compensate the low power of incident light, the exposure time was increased to 150 μs per single signal registration in all measurements.

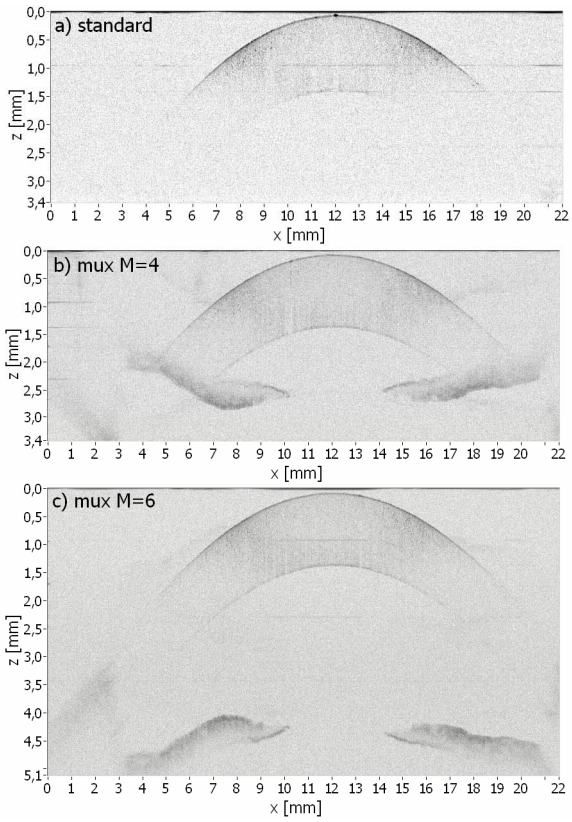

Fig. 10. Cross-sectional image of the anterior chamber of porcine eye *in vitro* obtained by a) standard SOCT, and multiplexing SOCT using OFC for b) $M = 4$ and c) $M = 6$.

Because of a postmortem changes in the porcine eye the crystalline lens is not visible in Fig. 10. Another experiment using multiplexing technique performed in other porcine eye enabled reconstruction of the entire anterior chamber with visible anterior surface of the crystalline lens (Fig. 11).

#92342 - $15.00 USD Received 31 Jan 2008; revised 1 Mar 2008; accepted 7 Mar 2008; published 12 Mar 2008

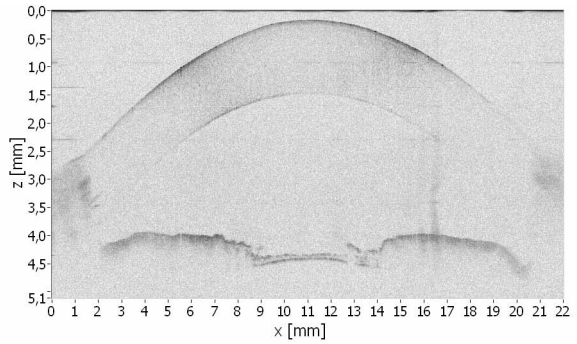

Fig. 11. Cross-sectional image of the anterior chamber of porcine eye *in vitro* obtained by multiplexing SOCT technique with $M = 6$. In this image the anterior surface of the crystalline lens is also visible.

6. Discussion

The technique presented in this contribution overcomes several limitations of high resolution SOCT such as limited imaging range, partial aliasing and sensitivity drop with depth what is demonstrated in Fig. 9, 10 and 11. The price to be paid for these improvements is *M*-fold increase in the measurement time. This inconvenience can be potentially reduced by replacing CCD cameras with CMOS photodetectors. In this case it is possible to read out a reduced number of pixels from the entire photosensitive array in proportionally shorter time. Therefore, the multiplexing method can be used in SOCT instruments comprising CMOS detectors without loosing measurement time. Further increase of the measurement time is due to considerable reduction of optical power caused by a F-P filter. This can be solved either by application of light sources with higher power and the Fabry-Perot interferometer or by employing an active OFC generator [33].

The multiplexing technique relies on shifting the comb by changing an air gap *d* in the Fabry-Perot interferometer what slightly influences its FSR. Because of that, the consecutive combs are not shifted in ideal parallel manner. The maximal deviation at the both edges of the spectrum reaches ±12 % of the pixel width. If a signal is sampled imperfectly in *k*-space, the artificial image repetitions appear after Fourier transformation. Since the effect is deterministic, it is corrected in the numerical post processing. However, due to the imperfections of numerical processing, the artifacts still remain and are visible in Fig. 10(b) and (c). Further improvement of the software and electrical stability of the driving system should effectively reduce this effect. Also a combination of uneven distribution of comb peaks onto the detector array and decreased sensitivity drop-off can cause the presence of double aliased images. Such an artifact can be visible in the Fig. 8 (b) as a part of the retinal structure in the low-frequency area of the cross-sectional image. This effect can be removed by careful adjustment of the spacing between the comb peaks (FSR of the Fabry-Perot interferometer) to superimpose the real and the double aliased images.

The image reconstruction in the presented method can be also affected by a sample motion. This is a common problem of methods based on multiple registration of the spectral fringe signals [25, 29, 34, 35]. Thus reduction of registration time in proposed method is indispensable to minimize motion artifacts. Relatively long repetition time was chosen to avoid influence of mechanical resonance close to 50 kHz observed in our FPI device. Firstly we had to increase the time constant of the electronics driving the FPI, then we had to delay the CCD camera trigger to ensure the FPI is relaxed within 99% of the final position – then the integration of light is proceed. Higher power of light on the object permits the appropriate reduction of the measurement time, which makes the requirement of object stability less difficult to fulfill.

In order to obtain very stationary comb over the exposure time, the Fabry-Perot filter is driven by a staircase signal. Because of high capacity of the F-P interferometer (2.2 μF) the

#92342 - $15.00 USD Received 31 Jan 2008; revised 1 Mar 2008; accepted 7 Mar 2008; published 12 Mar 2008

rising time of the signal increases the repetition time between consecutive spectra registration to 400 μs. This problem might be reduced either by improvements in the driving electronics.

It must be noted, that simple increase of number of detector pixels in standard SOCT will also theoretically increase imaging depth, but the accompanying dramatic loss of sensitivity would make this procedure impractical. The interpixel shift technique [30] solves the problem of partial aliasing, but it is also affected by considerable sensitivity drop. The presented method has the potential to increase the imaging range in more flexible manner – just by software control. In contrast, standard SOCT system needs hardware changes (reconstruction of a spectrometer), while the interpixel shift technique requires mechanical movement of the detector.

7. Conclusion

A novel Spectral Optical Coherence Tomography method using an Optical Frequency Comb (OFC) is demonstrated. This technique overcomes several limitations of high resolution SOCT. In the presented method an optical frequency comb is generated with a broadband light source and a Fabry-Perot interferometer. The optical comb can be shifted over the CCD detector by a fraction of one *FSR* to increase the effective number of samples of the signal. This allows increasing the imaging range with preserved high axial resolution. We presented preliminary data demonstrating the general performance, advantages and limitations of the multiplexing SOCT method using an optical frequency comb. High quality, high resolution cross-sectional images of biological samples with increased imaging range were obtained with the presented technique. It was demonstrated that the multiplexing technique expands imaging depth up to 5.1 mm of the SOCT system preserving 3.5 μm axial resolution over the entire depth. In result, the entire anterior chamber of porcine eye is imaged with a high level of details.

Acknowledgements

Authors of this paper would like to thank prof. Piotr Targowski, dr Zygmunt Turło and Bogdan Szymański for their help and support. This work was supported by Polish Ministry of Science, grants for years 2006/2009 and EURYI award. Maciej Wojtkowski acknowledges additional support of Foundation for Polish Science (Homing project) and Rector of NCU for the scientific grant 504-F. Authors would also like to thank Kevin Hsu from Micron Optics for his support. Robert Huber acknowledges support by the Emmy Noether program of the German Research Foundation (DFG, HU1006/2-1).

#92342 - $15.00 USD Received 31 Jan 2008; revised 1 Mar 2008; accepted 7 Mar 2008; published 12 Mar 2008